Electrochimica Acta 374 (2021) 137487

Contents lists available at ScienceDirect

Electrochimica Acta

journal homepage: www.elsevier.com/locate/electacta

In-operando Raman study of lithium plating on graphite electrodes of lithium ion batteries

M.A. Cabañero[a,*], M Hagen[b], E. Quiroga-González[c]

[a] Centre for Cooperative Research on Alternative Energies (CIC energiGUNE), Basque Research and Technology Alliance (BRTA), 01510 Vitoria-Gasteiz, Spain
[b] Fraunhofer Institute for Chemical Technology (ICT), 76327 Pfinztal, Germany
[c] Institute of Physics, Benemérita Universidad Autónoma de Puebla, 72570 Puebla, Mexico

ARTICLE INFO

Article history:
Received 22 September 2020
Revised 10 November 2020
Accepted 15 November 2020
Available online 18 November 2020

Keywords:
Lithium plating
Raman
Graphite anode
Li ion batteries
In-operando

ABSTRACT

In-operando Raman spectroscopy with high spatial resolution (1 μm^2) was employed to study the lithium deposition reaction on graphite electrodes. The 1850 cm^{-1} acetylide band, which is always found on lithium metal spectra, appeared right after reaching the full lithiation of graphite, when the G and D bands of graphite vanished. The band was observed during potestiostatic overcharge at high and low current rates and in a post-mortem analysis. The results suggest that during the constant voltage step, lithium is deposited and concurrently chemically intercalated into graphite. The second mechanism becomes the dominant after 30 min, when the current decreases. The evolution of the G and D bands of graphite and the lithium concentration in the electrolyte was also studied. The results suggest that EC is slowly consumed after the onset of lithium plating.

This work demonstrates the possibility of studying locally the lithium plating onset and chemical intercalation on the graphite electrodes in real time.

1. Introduction

Lithium ion batteries are the main component to improve, in order to achieve a widespread use of electric vehicles in the coming years contributing to a more sustainable mobility. Between the main drawbacks (challenges) of this technology, to be able to compete with the conventional internal combustion engine (ICE) vehicles, are: its lower energy density, higher cost, shorter lifetime, and lower safety. In order to improve the acceptance of the final user, it is also important that the charging time of electric vehicles reduces to less than 15 min. However, lithium plating is common during fast-charging, especially at low temperatures [1–3,55], and it is considered one of the main degradation phenomena of Li-ion batteries. Additionally, it represents a safety risk, since plating can grow in the form of dendrites that eventually can cause short-circuit; furthermore, short circuits produce an abrupt increase of temperature, burning the battery. This is the main safety issue of lithium ion batteries [4].

Different approaches have been followed to detect and quantify Lithium-plating. [3,5–11] Nevertheless, just a few of these techniques provides local information in real time [3,6,7,9,11,12]. On the other hand, since the formation of dendrites in metallic anodes arises faster than in intercalation compounds as graphite, most studies about dendrite growth and lithium plating are focused on lithium metal electrodes and just a few cover this problem on graphite electrodes. Lüders et al. have studied the variation of the lithiation in graphite by in-situ neutron diffraction on the complete cell, which indirectly provides information on the lithium deposition [3]. Wandt et al. employed a special cell to detect *in-operando* lithium plating by means of electron paramagnetic resonance (EPR) [11]. However, the spatial resolution of this technique is limited and it is not able to distinguish about the position where lithium is being deposited (i.e. within the electrode or as a dendrite that might punch the separator). In the recent work of Finegan et al. high speed synchrotron X-ray diffraction is employed to quantify spatially and in real time lithium deposition and the evolution of the graphite intercalation compounds. [12] The signal of metallic lithium with this technique is low which follows to reduced spatial resolution around 10 µm. In large format cells, where temperature and current distribution are inhomogeneous, lithium plating starts locally and is difficult to detect. Therefore, methods with high spatial resolution are needed in order to better understand this degradation mechanism and develop new measures for its mitigation.

Raman spectroscopy is a vibrational technique that provides unique information about the different organic and inorganic

* Corresponding author.
E-mail address: macabanero@cicenergigune.com (M.A. Cabañero).

https://doi.org/10.1016/j.electacta.2020.137487
0013-4686/

compounds in a material. For this reason, in the last decades, there are several reports on Raman spectroscopy on graphite electrodes, studying mainly the Li intercalation process [13–18], the SEI formation [14,19], the effect of electrolyte additives [20], the Li concentration in electrolyte [21], as well as its degradation [22,23]. In lithium metal anodes, a band at 1850 cm^{-1}, observed in different studies [24–27] has been assigned to lithium acetylide (Li_2C_2) [25]. This band was also observed on graphite electrodes when the potential was close to 0 V vs. Li/Li^+ [28,29]. A recent study by Fonseca et al. identified the same band as a lithium plating marker on overcharged graphite/NMC cells [30]. However, it was a post-mortem evaluation and the samples were measured ex-situ. Therefore, the onset conditions of lithium plating and its evolution during charging could not be evaluated.

In this work, we present the results of an in-operando Raman spectroscopy study of Li plating on graphite electrodes in half cells with Li metal as a counter electrode. The 1850 cm^{-1} acetylide band, appearing right after reaching the full lithiation of graphite (phase LiC_6), was used to track Li plating. This band grows steadily, while the G and D bands of graphite fade. This demonstrates the possibility of studying the lithium plating onset and its growth on graphite electrodes in real time. This was accomplished with high spatial resolution (1 μm^2). To the best of our knowledge, this is the first time that in-operando Raman was performed to study plating on graphite anodes. This result was also confirmed in a post-mortem study of graphite electrodes that underwent different levels of overcharge.

2. Experimental section

Raman spectra were collected using a Horiba Jobin Yvon HR800 spectrometer. The Raman spectrometer was equipped with a 532 nm laser and a CCD detector. The detector temperature was kept under 5 °C and a 0.3 filter was set for the laser. A x50 objective was employed in all the measurements, which means a multiplication of 1.4 × 100 the size of the image. Confocal analysis was performed with a spatial resolution of 1 × 1 µm, which lies within the size of a graphite particle (10 µm for the material under study).

The graphite electrodes under study were extracted from commercial cells (pouch type Model SLPB78216216H). Cells were open in a glove box under argon atmosphere. Samples were soaked in dimethyl carbonate (MERCK SelectyLite^{TM}) for 60 min, then the dimethyl carbonate solution was renewed, and the samples were soaked for another 30 min.

The cell configuration employed for the in-operando characterization by Raman spectroscopy has been reported in a previous work [31]. This configuration allows "in-operando" evaluation of the cells in standard electrode configuration (against each other), although just the electrode edges can be observed.

In-operando measurements were performed with graphite as working electrode and lithium metal as the counter electrode. The electrolyte employed was LP57 from BASF (1 M $LiPF_6$ in EC:EMC 3:7). The optical cell was fixed on the movable sample table with 0.1 µm accuracy. The optical microscope was used to select the measurement point. The spectra was recorded every 20 min during the graphite lithiation process. Measurements were taken first at the graphite surface and later at the lithium surface, always at the same electrode location (coordinates established in an automatic manner thanks to the microscope stage). Cells were cycled using a Ivium CompactStat Potentiostat.

The processing of the spectra was necessary as fluorescence was contributing to signal. First the background was removed by an adaptative algorithm AIRPLS described in the work from Zhang et al. [32]. Secondly, spikes were removed when necessary and the data were smoothed using the Savitzky-Golay filter with polynomial order 5 and 51 to 101 number of points depending on the noise of the spectra [33]. Finally, the spectra were normalized on the standard deviation of the spectra.

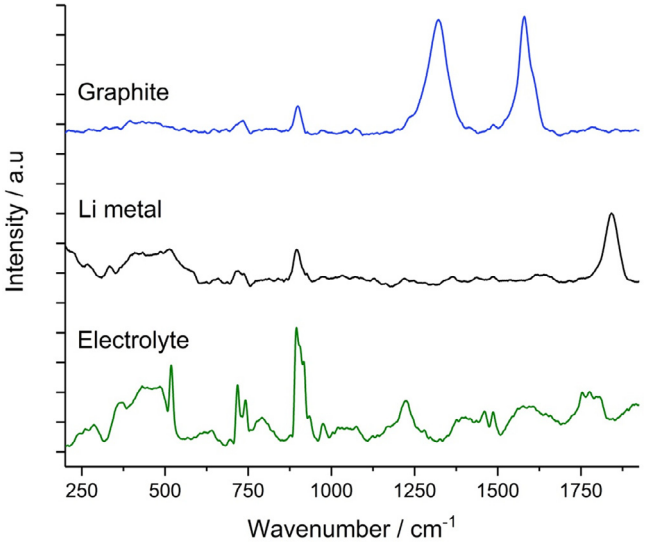

Fig. 1. Raman spectra of graphite electrode, lithium metal counter electrode and electrolyte.

The post-mortem study was performed on three half-cells (graphite vs. metallic lithium), where a first charge cycle at C/10 was applied (charged capacity in all cells of 1.15 mAh, which corresponds to the pouch cell capacity specified by the manufacturer). Then the cells were discharged until different overcharge percentages and then were disassembled in a glove box under inert atmosphere. The electrodes were not washed in order to avoid the removal of the SEI.

3. Results and discussion

Fig. 1 shows the Raman spectra of the graphite working electrode and the lithium metal counter electrode during the first lithiation process. In order to exclude which peaks were contributions from the 1 M $LiPF_6$ EC:EMC electrolyte, one spectrum was also recorded at the separator. The spectra have been processed as detailed in the experimental section to remove the contribution from the background. The majority of the peaks from the electrolyte spectra have been assigned to vibrational bands from the solvents EC or EMC. One of the main peaks from the $LiPF_6$ is also present at 741 cm^{-1}.

Table 1 summarizes the position of the bands, their origin, and references to other studies where they have been identified. The strong peaks of the electrolyte spectrum are attributed [34] to: EC non-solvated peaks at 718 cm^{-1} (C = O ring bending mode) and 894 cm^{-1} (O-C-O ring breathing), and EC-Li^+ solvated peaks at 730 cm^{-1} and 905 cm^{-1} and to EMC at 1223 cm^{-1} (CH_3-O). The EC solvated and non-solvated peaks were also measured in the spectra of both electrodes: graphite and lithium metal. The relative variation of the intensity between the solvated and non-solvated EC-Li^+ peaks, can be used to study the consumption of EC and to quantify the local Li ion concentration [21].

A broad peak around 450 cm^{-1} is also observed, which is also present with minor intensity in the spectrum of metallic lithium. Naudin et al. also reported this broad band at around 500 cm^{-1} which had different intensity depending on the position at the lithium metal electrode [24]. This could be due to an inhomogeneous SEI, as they ascribed this peak to Li_2O. The peak was also observed in the recent work of Fonseca et al. in the spectra of plated lithium on graphite electrodes [30]. Other weak peaks

Table 1
Position, assignment and references of the peaks of the spectra from electrolyte, graphite and metallic lithium electrode. s=strong, w=weak, m=medium, b=broad, v=very.

Position in Electrolyte spectra/cm^{-1}	*Position in Graphite spectra/cm^{-1}*	*Position in Li metal spectra/cm^{-1}*	*Assignement*	*Position in reference/cm^{-1}*	*Reference*
154 (w)	–	–	$LiOH•H_2O$	144	[35]
241 (w)	–	–	$LiOH•H_2O$	245	[35]
260 (w)	–	267(vw)	unknown	–	–
288 (w)	–	–	LiF	300	[36,37]
367 (w)	–	333 (m)	$LiOH•H_2O$	356	[35]
428–485 (b)	–	408–514 (s)	Li_2O	400–500	[24,37]
518 (s)	–	515 (w)	LiOH	525	[39]
695 (m)	–	–	EMC – ν_{OCO2}	695	[40]
718 (s)	713 (m)	716 (m)	EC– ν_{OCO}	717	[34,37,41]
741 (s)	734 (m)	736 (m)	$LiPF_6$	739	[42]
790 (b)	–	–	EMC – $\nu_{C=O}$	799	[40]
894 (s)	898 (m)	895 (m)	EC – ring breathing	894	[34,41]
975 (m)	973 (vw)	973 (vw)	EMC – $\nu_{C=O}$	974	[40]
1003–1075 (b)	1070 (vw)	1031 (vw)	Li_2CO_3	1071	[22,37,41]
1223 (s)	–	1219 (vw)	EMC – ν_{CH3-O}	1223	[40,41]
–	1319 (s)	1363 (m)	D band of Graphite	1350	[22]
1457 (m)	–	–	EMC– ν_{CH}	1461	[40]
1484 (m)	1486 (w)	1486 (w)	EC– ν_{CH2}	1484	[34,41]
1586 (b)	1586 (s)	1615–1640 (w,b)	G band of Graphite	1580	[22]
1753 (m)	–	–	EMC – $\nu_{C=O}$	1758	[40]
1774 (m)	–	–	EC– $\nu_{C=O}$	1773	[41]
1801 (m)			EC– $\nu_{C=O}$	1798	[41]
–	–	1850 (s)	Li_2C_2	1850	[24–26,37]

of the electrolyte's spectrum are products from the reaction with water such as lithium hydroxide monohydrate $LiOH•H_2O$ [35] or Li_2O from the counter electrode[24,36,37]. The narrow peak at 518 cm$^{-1,}$ assigned to LiOH by Hase et al. [38], is observed in both the electrolyte and the lithium metal electrode.

The Raman spectrum of lithium metal (black line) exhibits the characteristic peak at 1850 cm^{-1} which was attributed to the stretching of the triple bond of lithium carbide (Li_2C_2) by Schmitz et al. [26], and it is found in numerous studies of Raman spectroscopy of lithium metal electrodes [24–26,36,37]. Naudin et al. claimed that the formation of the Li_2C_2 and therefore the presence of this band is related to the laser irradiance (although only for $P > 1$ mW/μm^2) [24]. They claimed that Li_2CO_3 is first formed on the metallic lithium surface and the heating from the laser transforms it into Li_2C_2. On the contrary, the group from Schmitz et al. concluded that the band appears independently of the laser power employed, during the formation of the SEI and confirmed the presence of Li_2C_2 by mass spectroscopy [25]. In the recent work of Tang et al. [37] the band at 1850 cm^{-1} appears when a laser power of 0.1 mW is employed in very small quantities of Li deposited nanorods on Cu foil (200–300 nm diameter), but in case of high water content within the cell, the LiF in the SEI prevents the formation of Li_2C_2. One can conclude, that even with low laser power, it is possible to form Li_2C_2, probably due to the heating reached by prolonged exposure time. On the other hand, even when the sensitivity of raman is low, the signal measured from Li_2C_2 or other SEI elements is probably enhanced due to the surface-enhanced Raman scattering (SERS) effect [34,37].

In the spectrum of the lithium metal electrode of Fig. 1, the band at 518 cm^{-1} associated to LiOH is very weak. This suggests that the water content in our cell is very low. References to the broad peak at 500 cm^{-1} are also found in various Raman studies of lithium metal electrodes [24,37,39].

The Raman spectrum of the graphite electrode exhibits two main bands: the D and G-band, at 1319 and 1586 cm^{-1}, respectively. The D band is associated to the breakage of symmetry of the sp2 hybridization of the sheets of graphite, which takes place at the edge of the graphite sheets (with hybridization sp3). Band G comes from the graphitic ordering with hybridization sp2. Accordingly, the ratio between the D and the G band is associated to the carbon disorder. Large I_D/I_G ratios (tending to 1, for graphite) indicate a high degree of disorder. During the whole galvanostatic lithiation process of graphite at C/10 until 5 mV vs. Li/Li$^+$, the Li_2C_2 band at 1850 cm^{-1} does not appear on the graphite side, whereas is always present in the lithium metal spectra, which confirms its suitability to determine the onset for lithium metal deposition on graphite.

In order to detect the onset of the lithium plating reaction, the graphite anode was initially fully lithiated to 5 mV vs. Li/Li$^+$. In order to force the lithium plating reaction on the graphite electrode, an overcharge step was performed by keeping the potential at −5 mV vs. Li/Li$^+$. Note that Fig. 2 is based on the same dataset as the graphical abstract

Fig. 2a shows the spectra of the graphite electrode at different moments of the overcharge process. The D and G bands still exhibit considerable intensity at the beginning of the overcharge step, what indicates that the graphite particles under study are still not fully lithiated. The reason might be that no constant voltage step was performed during the lithiation to 5 mV or that the electrode is inhomogeneously lithiated; it is important to remember that the optical cell allows the measurement just at the cell edges.

Fig. 2b shows the area underlying the G-band during the overcharge process at −5 mV vs. Li/Li$^+$. Once the maximum value of the area of the G band is achieved (spectrum b), a continuous decrease follows until point c is reached. The broadening of the G band and its intensity fade upon lithiation have been already reported in other studies [16,18,43,44]. The increase in intensity during the first stages may be related to the focusing during the measurement due to changes of volume on graphite; it is important to mention that the z stage of the Raman microscope does not change during the measurements. After 20 min of lithiation (spectra d), the area corresponding to the G-band has almost vanished and the Li_2C_2 peak at 1850 cm^{-1} appears (point d in Fig. 2c).

The band assigned to the lithium carbide at 1850 cm^{-1} appears at the moment that the G-band peak fades due to full lithiation of graphite (spectra d and e), and is an indication of the onset of lithium plating on graphite. These results are in good agreement with the recent study of Fonseca Rodrigues et al. [30] where the presence of the Li_2C_2 at 1850 cm^{-1} was observed by post-mortem analysis, after overcharging a full cell: graphite vs. NMC. The de-

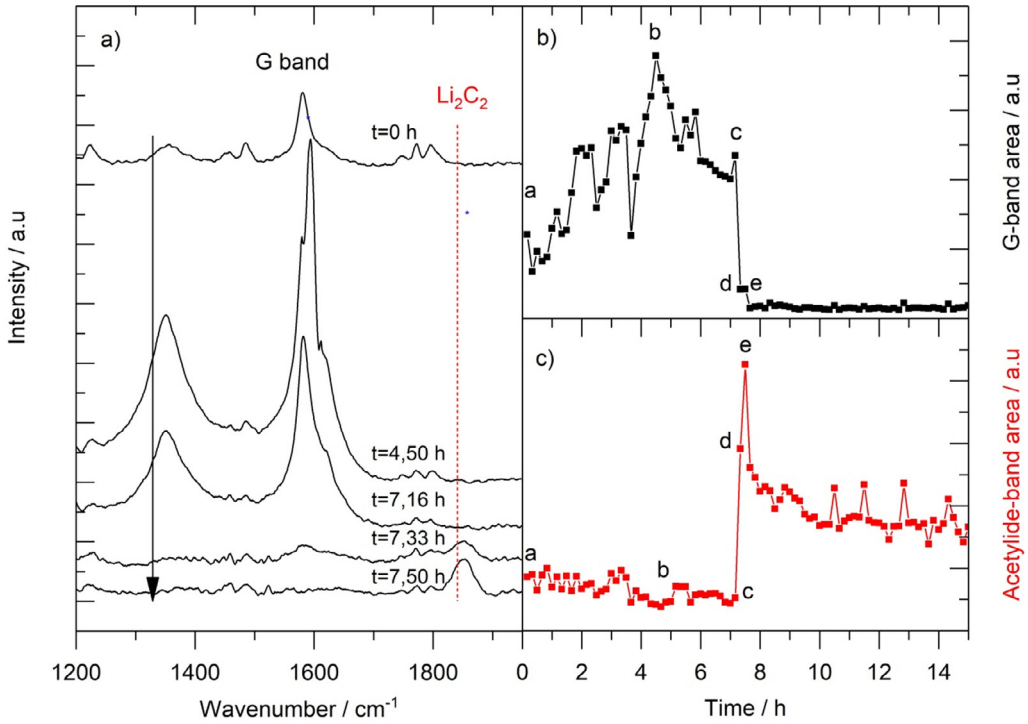

Fig. 2. a) Spectra of the graphite electrode during the first 8 h of overcharge until the lithium plating onset. Area of the G-band (b) and area of the Li_2C_2 band (c) vs. time during the whole overcharge process at constant voltage of −5 mV.

pletion of the G-band due to the full lithiation of graphite (formation of intercalation compounds with high Li content) has been reported in the literature [16].

The Li_2C_2 band at 1850 cm^{-1} reaches the maximum intensity after 20 min of overcharge (spectrum e) and afterwards it decreases due to chemical intercalation of the metallic lithium into the graphite when the current decreases during the CV step. Some local maxima appear during this period, related with the random nucleation of Lithium during plating (nature of electrochemical deposition, until a steady state is reached [45]<).

Higher rates of chemical intercalation than plating during the CV step at low current has been reported in different studies [12,46], and a fast chemical intercalation of the platted Li during the OCV step after charging has been widely revealed [2,3,11,47]. Bitzer and Gruhle measured a decrease of the cell thickness during the CV phase and it was identified as the point where the chemical intercalation of lithium on graphite is the dominant effect [46]. Finegan et al. measured with high-speed depth-profiling synchrotron X-ray diffraction (XRD) a decrease of the Li plating signal at the end of charging at 6C what they attributed to the faster rate of chemical intercalation vs. the rate of plating during the lower currents of the constant voltage step [12]. Lüders et al. determined that the chemical intercalation rate is independent on the quantity of lithium deposited [3]. The video from the Supplementary Information shows how in some particles the plated lithium is intercalated on graphite during a CV overchange step (change from gold coloured, LiC_6 to black coloured (lower lithiathion stages).

Fig. 3 shows the evolution of the G-band, the D-band, the non-solvated EC peak at 890 cm^{-1} (asterisks) and the solvated EC-Li^+ peak at 903 cm^{-1} (triangles) during the lithiation and overcharge process shown in Fig. 2. There are three zones defined by discontinuities in which the intensity of the G-band abruptly decreases after increasing almost linearly. The discontinuities could be caused by the redistribution of the intercalated Li ions in neighboring particles when a specific concentration is achieved (interparticle diffusion, see video from Supplementary Information). The Li^+ transport between particles was already observed by Harris et al. [48]. The EC and EC-Li^+ peaks at 890 and 905 cm^{-1}, associated to the local Li-ion concentration [21,28], follow the same trend that the G-band in the regions I-III. This is in agreement with the increase of the Li^+ concentration at the particles surface due to diffusion limitations, which then decreases when the Li ions are transported to neighboring particles.

The intensity of the D band, however, follows a smooth increasing trend with the time (zones I to III). Since the D band (A1g mode of graphite) is associated with the loss of symmetry at the edges of the graphite sheets, its intensity increment means that there are new openings at the cell edges in the particle zone under study. The intensity of the D-band decreases after zone III, what suggest that a high lithiation degree is achieved after zone III, following the same tendency than band G.

The I_D/I_G ratio increases slightly during intercalation until spectrum b is reached (see Fig. S2 of the Supplementary Information). At the end of the graphite lithiation, it decreases to its initial value. This indicates an increase on the graphite ordering at the end of the lithiation. Variations in the range of 0.5 for the I_D/I_G ratio were also observed by Sethuraman et al. [49] within a local region of 2 μm^2 thanks to Surface Raman Mapping of the graphite electrode.

After the beginning of the lithium deposition reaction (spectrum c), the EC and solvated EC-Li^+ peaks also reach their maximum (spectrum e) as well as the Li_2C_2 peak does, which is then followed by a decrease of the peak intensity. This is probably due to the increase of the Li ion concentration when the Li plating reaction starts and intercalation into the graphite is no longer possible. After this moment, the intensity of the EC-Li^+ spectrum increases vs. the EC spectrum, due to the consumption of EC during the formation of the SEI on the new deposited metallic lithium, as metallic lithium is very reactive with EC. An increase on the EC-Li^+ peak was also observed by Yamakana et al. due to EC consumption during the SEI formation [21]. Finally at the end of the overcharge step, the EC-Li^+ peak intensity follows a prompt increase of intensity when the current becomes zero. This behavior can be ex-

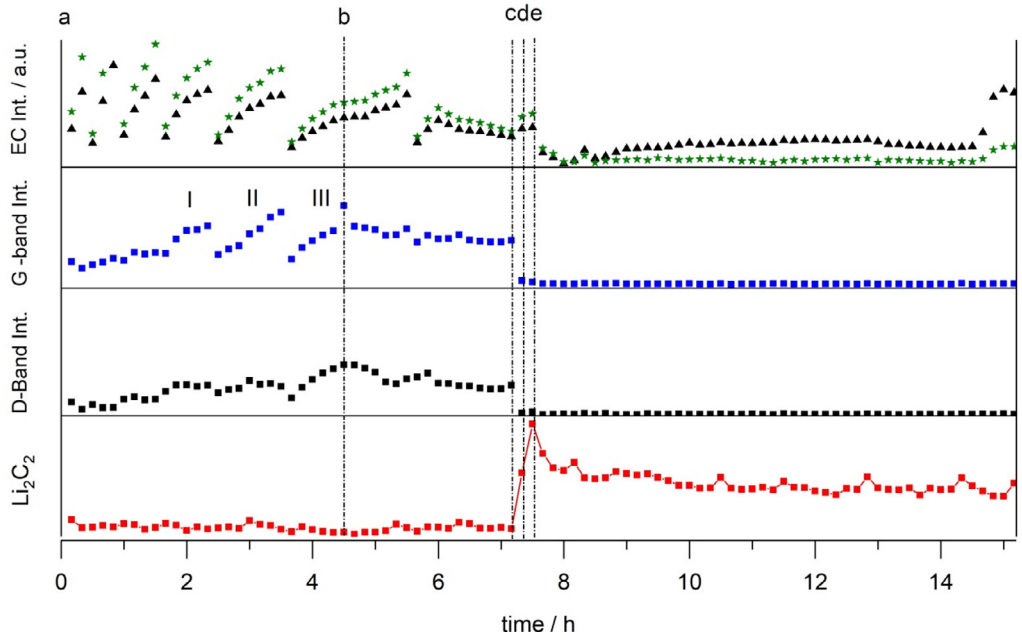

Fig. 3. Evolution of the intensities of bands G, D, EC at 890 cm^{-1}(asterisks) and solvated EC-Li+ at 905 cm^{-1} (triangles) and Li_2C_2 during the overcharge step at −5 mV. Capital letters defined specific zones of growing G-band intensity. Lower case identifies the spectra from Fig. 2a.

Table 2
Assignment of the Raman bands of the overcharged graphite electrode. s=strong, w=weak, m=medium, b=broad, v=very.

Overcharged Graphite spectra	*Assignement*	*Position in reference / cm^{-1}*	*References*
159 (s)	$LiOH•H_2O$	144	[35]
238 (s)	$LiOH•H_2O$	245	[35]
287 (m)	SEI, LiF	300	[36,37]
438–500 (s,b)	Li_2O	~ 500	[30]
478 (s)*	$LiPF_6$	470	[42]
602 (m)**	Li_3N	605	[39]
790 (s, b)**	$LiOH•H_2O$	840	[39]
1058 (m,b)**	Li_2CO_3	1072	[24]
1205 (w,b)	EMC	1215	[40]
1460 (w)*	Li_2CO_3	1440	[39]
1525 (w) *	ROCOOLi	1522	[51]
1765 (w)	EC or EMC	1773 or 1758	[41, 40]
1850 (s)*	Li_2C_2	1850	[24–26,37]
2434 (s)*	unknown		
2949 (w)**	water bound to LiOH and Li_3N	~2900	[39]

* Peak intensity varies with time.
** Peak intensity only decreases in the last spectrum, when $I = 0$.

plained by the dissolution of the Li ions in the electrolyte as they are no longer employed in the Li deposition reaction.

In order to evaluate the differences on the lithium deposition when the graphite is overcharged at high current densities, a half cell graphite vs. metallic lithium was first fully charged at C/2 (see Fig. 4a) up to −5 mV vs. Li/Li^+, and then the potential was kept constant until the current was below C/100. Then a galvanostatic step of 2C was applied for 3 h and a discontinuous potential variation was observed reaching up to −500 mV vs. Li/Li^+. The discontinuous potential is probably due to the formation of microshorts due to dendrite growth as has been observed in other overcharge studies [50]. After this discontinuity, the potential remains constant at about −50 mV vs. Li/Li^+. Once the lithium deposition on graphite at high C-rates was confirmed, a potentiostatic step at −5 mV was applied and the evolution of the Raman spectrum measured at the graphite electrode over time was followed (Fig. 4b). The peaks observed, their assignment and literature references are summarized in Table 2.

In Fig. S3 from the Supplementary Information, a strong and broad peak centered around 450 cm^{-1} was observed in the graphite spectrum. This peak was also observed in the spectrum of the electrolyte and of the lithium metal electrode (Fig. 1), although in this case its intensity is very high. This peak has been attributed to Li_2O by Naudin et al. [24] and was observed on the surface of metallic lithium in several works [30,37,52]. Besides that peak, other peaks of lower intensity, also attributed to LiOH [39], were detected at 159 cm^{-1}, 840 cm^{-1} and 2920 cm^{-1}. The strong intensities of some peaks associated to the SEI (Li_2CO_3 at 1460 cm^{-1}, R-COOLi at 1525 cm^{-1} and Li_2C_2 at 1850 cm^{-1}) indicates that the SEI possess a significant thickness after overcharging at high C-Rates compared to the one formed at lower C-Rates (Fig. 3). New peaks that were not observed in the spectrum of the graphite electrode plated at low C-Rate are the ones at 287 cm^{-1} and 600 cm^{-1} that have been attributed to LiF and Li_3N respectively [36,37,39].

Interestingly, the strong peaks of EC at 718 cm^{-1} and 894 cm^{-1} that were observed in the spectra of graphite and metallic lithium

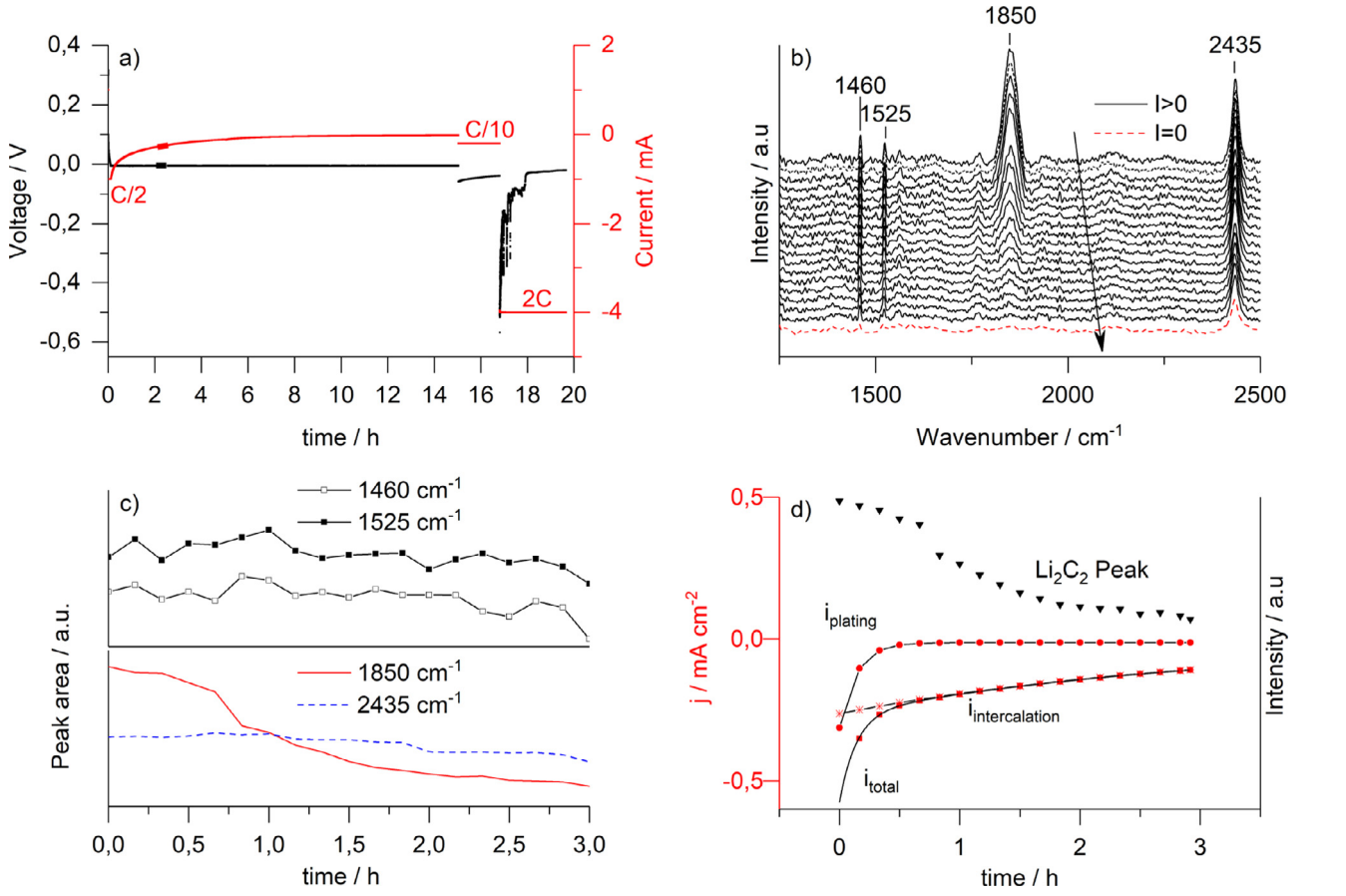

Fig. 4. a) Graphite electrode overcharge at high C-Rate, lithium deposition observed b) Graphite electrode spectra during potentiostatic overcharge step at E=−0.005 V after overcharge at high C-rate. c) Peak area variation of the Li_2CO_3 peak at 1460 cm^{-1}, R-COOLi at 1525 cm^{-1}, the Li_2C_2 peak at 1850 cm^{-1} and the unknown peak at 2435 cm^{-1} d) Li_2C_2 peak intensity and current evolution with time during the −5 mV step after overcharge at high C-rates. (For interpretation of the references to color in this figure, the reader is referred to the web version of this article.)

electrode during cycling (Fig. 1) and during lithium deposition at low C-rates (Fig. 3), are here very weak. The same behavior is observed with other bands associated to EMC or EC. This might be due to the electrolyte consumption due to the massive SEI growth on the metallic lithium.

When a potential of −5 mV vs. Li/Li^+ is applied, the only peaks that show a variation of intensity with the time are the ones at the following positions: 478 cm^{-1} ($LiPF_6$), 1460 cm^{-1} (Li_2CO_3), 1525 cm^{-1} (R-OCO_2Li), 1850 cm^{-1} (Li_2C_2) and 2435 cm^{-1} (non-identified), marked in Fig. 4b. Some peaks show just a small intensity decrease in the last spectra when the current is almost zero (see red dashed line in Fig. 4b). These are all bands attributed to some lithium compound: LiOH at 790 cm^{-1} and 2900 cm^{-1}, Li_3N at 600 cm^{-1} and Li_2CO_3 at 1058 cm^{-1}.

Fig. 4c shows the evolution with time of the four peaks that vary during overcharge in potentiostatic conditions. They all follow a decrease of their area over time, due to the current decrease during the potentiostatic step. This variation is stronger in the case of Li_2C_2, medium for the band at 2435 cm^{-1} and lower for Li_2CO_3 and R-COOLi. The non-identified peak at 2435 cm^{-1} has still considerable intensity when the current is close to zero (see dashed line in Fig. 4b). In the Raman studies of lithium metal or graphite electrodes where the 1850 cm^{-1} peak was observed, the measurement range was usually below 2000 cm^{-1}. This band may be associated to a decomposition product of the electrolyte.

The current curve has been fitted with two exponential contributions as expressed by Eq. (1). This can be attributed to the two simultaneous reactions taking place during overcharge: metallic lithium deposition and chemical intercalation of Li ions to graphite [3]. The value for parameters B_1 and B_2 is 0.002 s^{-1} and 0.0001 s^{-1} respectively. As the intensity of the Li_2C_2 peak is decreasing, the chemical intercalation into the graphite is the leading mechanism B_1=0.002 s^{-1}. The lithium plating current (B2=0.0001 s^{-1} in Eq. (1)) is almost negligible after 30 min of charge (see Fig. 4d), which would explain the decaying trend of the Li_2C_2 peak after 40 min (as the chemical intercalation of the plated lithium becomes the main mechanism and there is almost any new lithium plating being deposited). The current evolution has been fitted by the following equation, being A_1=−3.11 10^{-4} A cm^{-2}, A_2=−2.50 10^{-4} A cm^{-2}

$$\boldsymbol{j = A_1 + e^{-B_1 t} + A_2 + e^{-B_2 t}} \quad (1)$$

Finally, an overcharge study was performed on graphite vs. lithium cells after charging with 1C at constant current, which is the recommended rate for full charging of commercial lithium ion cells. This time, no constant voltage step was included. Initially the cells were galvanostatically charged at low rate i.e. C/10 up to 15 mV vs. Li/Li^+ to ensure that the graphite electrode reaches a high lithiation degree, and then a charge step followed until different overcharge percentages (calculated taking into account the capacity of the pouch cell according to the manufacturer, 1.15 mAh cm^{-2}) were reached: cell C: 16%, cell B: 35% and cell A: 66%. Right after, the cells were disassembled and an ex-situ Raman analysis, putting the graphite electrodes between two thin glass plates sealed with grease, was performed. Due to the different contact resistances of the cells and polarization of the counter electrode [53], large variations of the initial overpotentials were observed between cells (see Fig. 5c). In the case of cell A, despite of presenting a lower initial

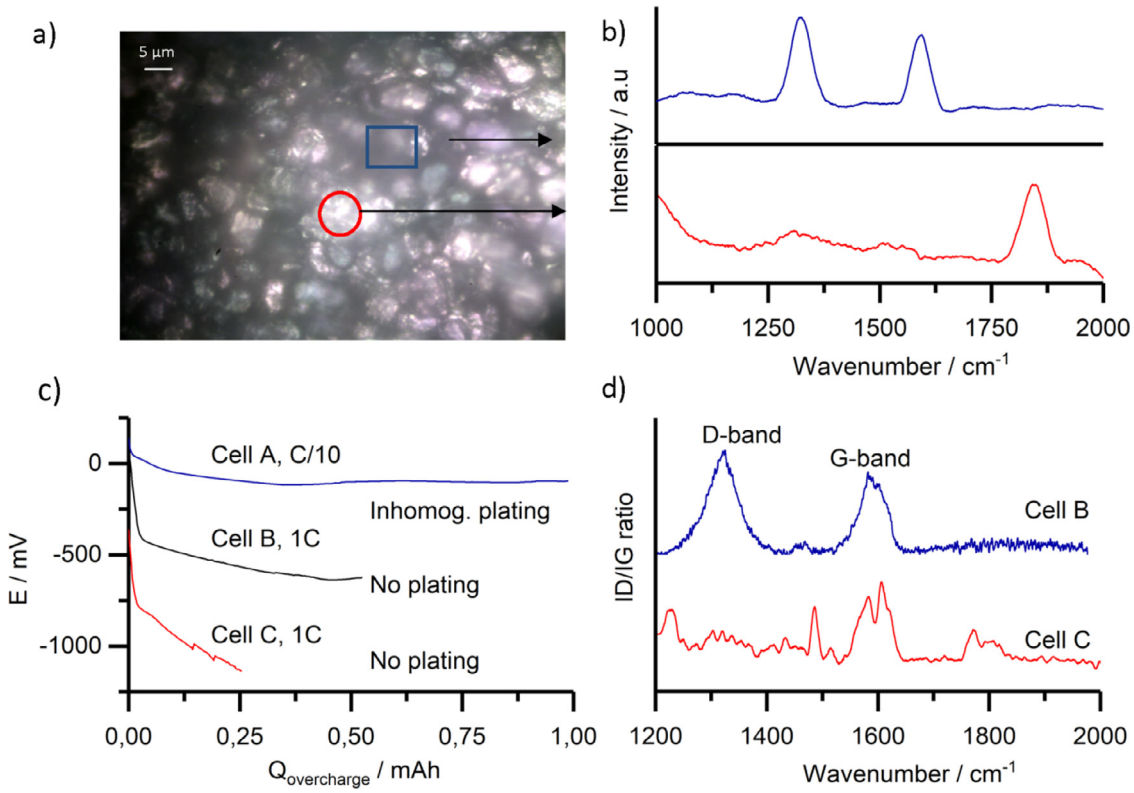

Fig. 5. a) Optical microscope image of the graphite electrode after constant current (CC) overcharge at 1. b) Spectra at two points of the graphite electrode from cell A with different lithiation grades: spot without lithium plating (blue line, taken at the blue rectangle area, graphite bands observed) spot with lithium plating (red line, taken at the red circle area, Li_2C_2 band observed) c) Potential evolution of graphite vs. Li of the three cells overcharged with CC up to different % of their capacity d) Spectra of the graphite electrode from cell B and C. (For interpretation of the references to color in this figure legend, the reader is referred to the web version of this article.)

overpotential due to the lower overcharge current (C/10), the Li_2C_2 mark at 1850 cm^{-1} was found at some specific spots (red circle of Fig. 5a). The lithium deposition on this cell is inhomogeneous, as a neighbor particle (blue rectangle in Fig. 5a) still exhibits the graphite D and G-bands and there is no Li_2C_2 evidence. The I_D/I_G ratio of this spectrum is 1.25 which is equal to the value found at some spots of cell B, and higher than in the study at low C-Rates from Fig. 3 (maximum I_D/I_G reached of 0.65). This indicates that the graphite reaches more disordered structures when charging at high C-Rates despite of the presence of lithium plating at some local spots. In cell B, no mark for lithium deposition was found, although very low potentials were achieved (−500 mV vs. Li/Li^+). As explained in the recent work from Zhang [53], the measured potential in a half-cell lithium metal vs. graphite is far from the real potential of graphite (difference of 50 mV at 1 C and up to 200 mV at 5C). If the contact resistance of the cell is high, this difference could be even more pronounced. The Li_2C_2 mark was not identified in cell C either, despite the low potentials measured. If we consider that the lithium deposition process starts only when the plateau below 0 V vs. Li/Li^+ is observed, the plated capacity on cell B was just 0.075 mAh and no Li is deposited on cell C as the plateau is not observed. Due to the relaxation process until the cell was open (one hour), this small quantity of plated lithium on cell B could have been intercalated in the graphite electrode. Such intercalation processes in the open circuit state have been reported in other studies [3]. The G-band is divided into two components in the spectra of cell B and cell C (see Fig. 5d). In cell B the two peaks are located at 1582 cm^{-1} and 1600 cm^{-1} and the D-band appears at 1325 cm^{-1}. In cell C the second peak is shifted to 1606 cm^{-1} and a new 1417 cm^{-1} (D0 band) appears, what has been reported in the case of carbonaceous materials of finite crystal sizes, which are imperfections rich [54]. The D-band at 1325 cm^{-1} is of very low intensity in cell C, as it has been reported in previous works (where it tends to disappear with Li intercalation) [14,18]. The shift of the G band to higher wavenumbers suggests that a higher lithiation degree was achieved in cell C.

4. Conclusions

In this work in-operando Raman spectroscopy was applied to study the lithium plating onset on graphite electrodes in half cells, using lithium metal as counter electrode. The results show that the peak attributed to lithium carbide (SEI component always found on the lithium metal spectra) at 1850 cm^{-1} appears when the peaks of the graphite D and G bands vanish due to full lithiation. This confirms the hypothesis from a previous post-mortem study where the peak was found on overcharged graphite electrodes. In addition to this, the peak intensity during an overcharge step in potentiostatic conditions (CV step) follows a decreasing behavior which indicates that the chemical intercalation on graphite takes places concurrently with lithium deposition and that the first one is the dominant effect when the current is low at the end of the CV step.

Consequently, in-operando Raman spectroscopy can be employed to study the evolution of the lithium deposition reaction. The lithium plating mark has been observed at different charge conditions: with high and low current densities in galvanostatic and potentiostatic measurements. A new band at 2440 cm^{-1} was also identified, which also followed a decreasing trend during the potentiostatic step. It could be assigned to a degradation product from the electrolyte or a SEI compound formed on metallic lithium.

After charging the cell with 1C rate, inhomogeneous lithiation/plating was found at different electrode positions. Differences on the particle size, porosity and thickness among others can lead

to this effect. Thanks to the high spatial resolution of 1 μm^2 of this technique, the influence of these factors can be further explored.

Declaration of Competing Interest

The authors declare that they have no known competing financial interests or personal relationships that could have appeared to influence the work reported in this paper.

Credit authorship contribution statement

M.A. Cabañero: Conceptualization, Software, Investigation, Data curation, Writing - original draft, Visualization. **M Hagen:** Methodology, Resources. **E. Quiroga-González:** Validation, Resources, Writing - review & editing, Supervision.

Acknowledgments

Funding through the Fraunhofer Project Group Electrochemical Energy Storage, received from the Bavarian State Ministry of Economic Affairs and Media, Energy and Technology is gratefully acknowledged.

Supplementary materials

Supplementary material associated with this article can be found, in the online version, at doi:10.1016/j.electacta.2020.137487.

Reference

[1] T. Waldmann, M. Wilka, M. Kasper, M. Fleischhammer, M. Wohlfahrt-Mehrens, Temperature dependent ageing mechanisms in Lithium-ion batteries – A Post–Mortem study, J. Power Sources 262 (2014) 129–135.
[2] J. Fan, On the discharge capability and its limiting factors of commercial 18650 Li-ion cell at low temperatures, J. Power Sources 117 (2003) 170–178.
[3] C. von Lüders, V. Zinth, S.V. Erhard, P.J. Osswald, M. Hofmann, R. Gilles, A. Jossen, Lithium plating in lithium-ion batteries investigated by voltage relaxation and in situ neutron diffraction, J. Power Sources 342 (2017) 17–23.
[4] G. Pistoia, Batteries for Portable Devices, 1st ed., Elsevier, Amsterdam, Oxford, New York, 2005.
[5] D. Anseán, M. Dubarry, A. Devie, B.Y. Liaw, V.M. García, J.C. Viera, M. González, Operando lithium plating quantification and early detection of a commercial LiFePO4 cell cycled under dynamic driving schedule, J. Power Sources 356 (2017) 36–46.
[6] J.-.H. Cheng, A.A. Assegie, C.-.J. Huang, M.-.H. Lin, A.M. Tripathi, C.-.C. Wang, M.-.T. Tang, Y.-.F. Song, W.-.N. Su, B.J. Hwang, Visualization of Lithium Plating and Stripping via in Operando Transmission X-ray Microscopy, J. Phys. Chem. C 121 (2017) 7761–7766.
[7] M.V. Avdeev, A.A. Rulev, V.I. Bodnarchuk, E.E. Ushakova, V.I. Petrenko, I.V. Gapon, O.V. Tomchuk, V.A. Matveev, N.K. Pleshanov, E.Y. Kataev, L.V. Yashina, D.M. Itkis, Monitoring of lithium plating by neutron reflectometry, Appl. Surf. Sci. 424 (2017) 378–382.
[8] N. Harting, N. Wolff, U. Krewer, Identification of Lithium Plating in Lithium-Ion Batteries using Nonlinear Frequency Response Analysis (NFRA), Electrochim. Acta 281 (2018) 378–385.
[9] Q. Li, T. Yi, X. Wang, H. Pan, B. Quan, T. Liang, X. Guo, X. Yu, H. Wang, X. Huang, L. Chen, H. Li, In-situ visualization of lithium plating in all-solid-state lithium-metal battery, Nano Energy 63 (2019) 103895.
[10] T. Waldmann, B.-.I. Hogg, M. Wohlfahrt-Mehrens, Li plating as unwanted side reaction in commercial Li-ion cells – A review, J. Power Sources 384 (2018) 107–124.
[11] J. Wandt, P. Jakes, J. Granwehr, R.-.A. Eichel, H.A. Gasteiger, Quantitative and time-resolved detection of lithium plating on graphite anodes in lithium ion batteries, Mater. Today 21 (2018) 231–240.
[12] D.P. Finegan, A. Quinn, D.S. Wragg, A.M. Colclasure, X. Lu, C. Tan, T.M.M. Heenan, R. Jervis, D.J.L. Brett, S. Das, T. Gao, D.A. Cogswell, M.Z. Bazant, M. Di Michiel, S. Checchia, P.R. Shearing, K. Smith, Spatial dynamics of lithiation and lithium plating during high-rate operation of graphite electrodes, Energy Environ. Sci. 13 (2020) 2570–2584.
[13] J. Zou, C. Sole, N.E. Drewett, M. Velický, L.J. Hardwick, In Situ Study of Li Intercalation into Highly Crystalline Graphitic Flakes of Varying Thicknesses, J. Phys. Chem. Lett. 7 (2016) 4291–4296.
[14] S. Pérez-Villar, P. Lanz, H. Schneider, P. Novák, Characterization of a model solid electrolyte interphase/carbon interface by combined in situ Raman/Fourier transform infrared microscopy, Electrochim. Acta 106 (2013) 506–515.
[15] H. Nakagawa, Y. Domi, T. Doi, M. Ochida, S. Tsubouchi, T. Yamanaka, T. Abe, Z. Ogumi, In situ Raman study on degradation of edge plane graphite negative-electrodes and effects of film-forming additives, J. Power Sources 206 (2012) 320–324.
[16] Y. Luo, W.-.B. Cai, D.A. Scherson, In Situ, Real-Time Raman Microscopy of Embedded Single Particle Graphite Electrodes, J. Electrochem. Soc. 149 (2002) A1100.
[17] C.M. Julien, A. Mauger, In situ Raman analyses of electrode materials for Li-ion batteries, AIMS Mater. Sci. 5 (2018) 650–698.
[18] P. Lanz, P. Novák, Combined In Situ Raman and IR Microscopy at the Interface of a Single Graphite Particle with Ethylene Carbonate/Dimethyl Carbonate, J. Electrochem. Soc. 161 (2014) A1555–A1563.
[19] S. Hy Felix, Y.-.H. Chen, J.-y. Liu, J. Rick, B.-.J. Hwang, In situ surface enhanced Raman spectroscopic studies of solid electrolyte interphase formation in lithium ion battery electrodes, J. Power Sources 256 (2014) 324–328.
[20] S. Maruyama, T. Fukutsuka, K. Miyazaki, T. Abe, In situ Raman spectroscopic analysis of solvent co-intercalation behavior into a solid electrolyte interphase-covered graphite electrode, J. Appl. Electrochem. 49 (2019) 639–646.
[21] T. Yamanaka, H. Nakagawa, S. Tsubouchi, Y. Domi, T. Doi, T. Abe, Z. Ogumi, Correlations of concentration changes of electrolyte salt with resistance and capacitance at the surface of a graphite electrode in a lithium ion battery studied by in situ microprobe Raman spectroscopy, Electrochim. Acta 251 (2017) 301–306.
[22] R. Kostecki, F. McLarnon, Microprobe study of the effect of Li intercalation on the structure of graphite, J. Power Sources 119-121 (2003) 550–554.
[23] E. Markervich, G. Salitra, M.D. Levi, D. Aurbach, Capacity fading of lithiated graphite electrodes studied by a combination of electroanalytical methods, Raman spectroscopy and SEM, J. Power Sources 146 (2005) 146–150.
[24] C. Naudin, J.L. Bruneel, M. Chami, B. Desbat, J. Grondin, J.C. Lassègues, L. Servant, Characterization of the lithium surface by infrared and Raman spectroscopies, J. Power Sources 124 (2003) 518–525.
[25] R. Schmitz, R. Ansgar Müller, R. Wilhelm Schmitz, C. Schreiner, M. Kunze, A. Lex-Balducci, S. Passerini, M. Winter, SEI investigations on copper electrodes after lithium plating with Raman spectroscopy and mass spectrometry, J. Power Sources 233 (2013) 110–114.
[26] R. Schmitz, R. Müller, S. Krüger, R.W. Schmitz, S. Nowak, S. Passerini, M. Winter, C. Schreiner, Investigation of lithium carbide contamination in battery grade lithium metal, J. Power Sources 217 (2012) 98–101.
[27] P.C. Howlett, D.R. MacFarlane, A.F. Hollenkamp, A sealed optical cell for the study of lithium-electrode|electrolyte interfaces, J. Power Sources 114 (2003) 277–284.
[28] P. Novák, F. Joho, R. Imhof, J.-.C. Panitz, O. Haas, In situ investigation of the interaction between graphite and electrolyte solutions, J. Power Sources 81-82 (1999) 212–216.
[29] J.-.C. Panitz, F. Joho, P. Novak, In Situ Characterization of a Graphite Electrode in a Secondary Lithium-Ion Battery Using Raman Microscopy, Appl. Spectrosc. 53 (1999) 1188–1199.
[30] M.-.T. Fonseca Rodrigues, V.A. Maroni, D.J. Gosztola, K.P.C. Yao, K. Kalaga, I.A. Shkrob, D.P. Abraham, Lithium Acetylide: A Spectroscopic Marker for Lithium Deposition During Fast Charging of Li-Ion Cells, ACS Appl. Energy Mater. 2 (2019) 873–881.
[31] M. Hagen, P. Schiffels, M. Hammer, S. Dörfler, J. Tübke, M.J. Hoffmann, H. Althues, S. Kaskel, In-Situ Raman Investigation of Polysulfide Formation in Li-S Cells, J. Electrochem. Soc. 160 (2013) A1205–A1214.
[32] Z.-.M. Zhang, S. Chen, Y.-.Z. Liang, Baseline correction using adaptive iteratively reweighted penalized least squares, Analyst 135 (2010) 1138–1146.
[33] A. Savitzky, M.J.E. Golay, Smoothing and Differentiation of Data by Simplified Least Squares Procedures, Anal. Chem. 36 (1964) 1627–1639.
[34] N. Mozhzhukhina, E. Flores, R. Lundström, V. Nyström, P.G. Kitz, K. Edström, E.J. Berg, Direct Operando Observation of Double Layer Charging and Early Solid Electrolyte Interphase, J. Phys. Chem. Lett. 11 (2020) 4119–4123.
[35] G. Li, H. Li, Y. Mo, L. Chen, X. Huang, Further identification to the SEI film on Ag electrode in lithium batteries by surface enhanced Raman scattering (SERS), J. Power Sources 104 (2002) 190–194.
[36] T.A. Galloway, L. Cabo-Fernandez, I.M. Aldous, F. Braga, L.J. Hardwick, Shell isolated nanoparticles for enhanced Raman spectroscopy, Faraday Discuss. 205 (2017) 469–490.
[37] S. Tang, Y. Gu, J. Yi, Z. Zeng, S.-.Y. Ding, J.-.W. Yan, D.-.Y. Wu, B. Ren, Z.-.Q. Tian, B.-.W. Mao, An electrochemical surface-enhanced Raman spectroscopic study on nanorod-structured lithium prepared by electrodeposition, J. Raman Spectrosc. 47 (2016) 1017–1023.
[38] Y. Hase, I.V. Pagotto Yoshida, The Raman active vibrational modes and isotopic effects of four isotopically substituted lithium hydroxides, Chem. Phys. Lett. 65 (1979) 46–49.
[39] A. Kumar, T.M. Arruda, A. Tselev, I.N. Ivanov, J.S. Lawton, T.A. Zawodzinski, O. Butyaev, S. Zayats, S. Jesse, S.V. Kalinin, Nanometer-scale mapping of irreversible electrochemical nucleation processes on solid Li-ion electrolytes, Sci. Rep. 3 (2013) 1621.
[40] L. Doucey, M. Revault, A. Lautié, A. Chaussé, R. Messina, A study of the Li/Li+ couple in DMC and PC solvents Part 1: Characterization of LiAsF6/DMC and LiAsF6/PC solutions, Electrochim. Acta 44 (1999) 2371–2377.
[41] B. Fortunato, P. Mirone, G. Fini, A. Spectrochimica Acta Part, Infrared and Raman spectra and vibrational assignment of ethylene carbonate, Mol. Spectrosc. 27 (1971) 1917–1927.
[42] R. Aroca, M. Nazri, G.A. Nazri, A.J. Camargo, M. Trsic, Vibrational Spectra and Ion-Pair Properties of Lithium Hexafluorophosphate in Ethylene Carbonate Based Mixed-Solvent Systems for Lithium Batteries, J. Solut. Chem. 29 (2000) 1047–1060.

[43] S. Migge, G. Sandmann, D. Rahner, H. Dietz, W. Plieth, Studying lithium intercalation into graphite particles via in situ Raman spectroscopy and confocal microscopy, J. Solid State Electrochem. 9 (2005) 132–137.
[44] M. Inaba, In situ Raman Study of Electrochemical Lithium Insertion into Mesocarbon Microbeads Heat-Treated at Various Temperatures, J. Electrochem. Soc. 143 (1996) 2572.
[45] O. Tobail, E. Quiroga-González, J. Carstensen, H. Föll, Enhancement of Cu Filling into p-Type Macro-Porous Silicon by Pore Wall Thinning, Oxide Deposition and Back Side Illumination, J. Electrochem. Soc. 161 (2014) D657–D662.
[46] B. Bitzer, A. Gruhle, A new method for detecting lithium plating by measuring the cell thickness, J. Power Sources 262 (2014) 297–302.
[47] V. Zinth, C. von Lüders, M. Hofmann, J. Hattendorff, I. Buchberger, S. Erhard, J. Rebelo-Kornmeier, A. Jossen, R. Gilles, Lithium plating in lithium-ion batteries at sub-ambient temperatures investigated by in situ neutron diffraction, J. Power Sources 271 (2014) 152–159.
[48] S.J. Harris, A. Timmons, D.R. Baker, C. Monroe, Direct in situ measurements of Li transport in Li-ion battery negative electrodes, Chem. Phys. Lett. 485 (2010) 265–274.
[49] V.A. Sethuraman, L.J. Hardwick, V. Srinivasan, R. Kostecki, Surface structural disordering in graphite upon lithium intercalation/deintercalation, J. Power Sources 195 (2010) 3655–3660.
[50] D. Ren, X. Feng, L. Lu, X. He, M. Ouyang, Overcharge behaviors and failure mechanism of lithium-ion batteries under different test conditions, Appl. Energy 250 (2019) 323–332.
[51] H. Wang, K. Xie, Investigation of oxygen reduction chemistry in ether and carbonate based electrolytes for Li–O2 batteries, Electrochim. Acta 64 (2012) 29–34.
[52] R.A.B. Álvarez, M. Cortez-Valadez, R. Britto-Hurtado, L.O.N. Bueno, N.S. Flores-Lopez, A.R. Hernández-Martínez, R. Gámez-Corrales, R. Vargas-Ortiz, J.-.G. Bocarando-Chacon, H. Arizpe-Chavez, M. Flores-Acosta, Raman scattering and optical properties of lithium nanoparticles obtained by green synthesis, Vib. Spectrosc. 77 (2015) 5–9.
[53] S.S. Zhang, Is Li/Graphite Half-Cell Suitable for Evaluating Lithiation Rate Capability of Graphite Electrode? J. Electrochem. Soc. 167 (2020) 100510.
[54] H. Nakagawa, Y. Domi, T. Doi, M. Ochida, S. Tsubouchi, T. Yamanaka, T. Abe, Z. Ogumi, In situ Raman study on the structural degradation of a graphite composite negative-electrode and the influence of the salt in the electrolyte solution, J. Power Sources 236 (2013) 138–144.
[55] Maria Angeles Cabañero Martínez, Investigation of the temperature dependence of lithium plating onset conditions in commercial Li-ion batteries, Energy 171 (2019) 1217–1228, doi:10.1016/j.energy.2019.01.017.